Journal of Molecular Structure 1298 (2024) 137010

Contents lists available at ScienceDirect

Journal of Molecular Structure

journal homepage: www.elsevier.com/locate/molstr

Structural characterization of a 3-hydroxychromone dye trehalose conjugate for fluorescent labelling of mycobacteria☆

Adrian Richter [a], Richard Goddard [b], Lea Mann [a], Fabienne Siersleben [a], Rüdiger W. Seidel [a,*]

[a] Institut für Pharmazie, Martin-Luther-Universität Halle-Wittenberg, Wolfgang-Langenbeck-Straße 4, 06120 Halle (Saale), Germany
[b] Max-Planck-Institut für Kohlenforschung, Kaiser-Wilhelm-Platz 1, 45470 Mülheim an der Ruhr, Germany

ARTICLE INFO

Keywords:
3-hydroxychromone
Dye trehalose conjugate
Crystal structure
Solvatochromic probe
Mycobacteria

ABSTRACT

3-Hydroxychromone (3HC) dye trehalose conjugates have previously been exploited as environment-sensitive fluorescent labels to detect mycobacteria by fluorescence microscopy. We have studied the 3HC dye 2-(6-(diethylamino)benzofuran-2-yl)-3-hydroxy-4*H*-chromen-4-one (**3HC-2**) trehalose conjugate **3HC-2-Tre** by X-ray crystallography, spectroscopic methods augmented by DFT calculations and conducted preliminary labelling experiments with *Mycobacterium abscessus*, a non-tuberculous mycobacterium and opportunistic pathogen. In the crystal structure of **3HC-2-Tre** · 3.14 H_2O, the **3HC-2-Tre** molecules exhibit an intramolecular O—H···O hydrogen bond between the 5-hydroxy group of trehalose and the chromone carbonyl oxygen atom, and form hydrogen-bonded dimers via the trehalose units with approximate local C_2 symmetry. The chromophore adopts an *s-cis* conformation of the chromone and benzofuran systems about its central C—C bond, as previously encountered in the crystal structure of the free dye **3HC-2**, and the trehalose moieties approximately retain the shape as found in the crystal structures of anhydrous trehalose and the dihydrate. Absorption spectra of **3HC-2-Tre** acquired in four different solvents revealed small positive solvatochromy. Fluorescence microscopy detected *M. abscessus* cells treated with **3HC-2-Tre** in the GFP channel.

1. Introduction

Tuberculosis (TB) is one of the most lethal bacterial infectious diseases in the world and continues to be a serious threat to public health. In 2021, an estimated 1.6 million people died of TB globally [1]. The pathogen causing TB is usually *Mycobacterium tuberculosis* [2]. The infection primarily manifests itself as a pulmonary disease but the bacteria can also invade other sites in the body, leading to extrapulmonary TB [3,4]. Non-tuberculous mycobacteria (NTM), i.e. those that cause neither TB nor leprosy, are also increasingly recognized as opportunistic pathogens in humans [5]. NTM infections likewise most commonly affect the lungs, thus resembling pulmonary TB, but can also occur as extrapulmonary infections, including skin and soft-tissue infections [6,7]. Certain patient groups, such as those with pre-existing structural lung diseases (e.g. cystic fibrosis or bronchiectasis) or a suppressed immune system, are at particular risk of developing NTM pulmonary disease [8].

To combat and prevent mycobacterial infections, early and rapid detection of the pathogens is important. Microscopy-based methods are particularly attractive in a low-resource environment [9]. In this context, Kamariza et al. reported a bright solvatochromic 3-hydroxychromone (3HC) dye trehalose conjugate that specifically detects *M. tuberculosis* within minutes [10]. 3HC dyes exhibit high fluorescence quantum yields and shifts in fluorescence intensity that are dependent on the polarity of the medium [11,12]. When bound to trehalose, the fluorophore is rapidly incorporated into the mycobacterial cell wall (Fig. 1). The antigen 85 (Ag85) enzymes that mycoloylate exogenous trehalose molecules in position 6 seem to tolerate an attached fluorophore. Upon insertion of the dye into the non-polar environment of the mycomembrane, fluorescence is turned on, and this property can be exploited for detection of mycobacteria with a fluorescence microscope. Aside from utilization for diagnostics and drug discovery [13–16], research applications of trehalose-based probes, such as the study of the dynamics of mycomembrane biosynthesis and remodelling, have also been described [17].

We became interested in fluorescent probes for labelling of viable mycobacterial cells as a possible tool for in vitro testing of anti-mycobacerial drug candidates. Recently, we reported on the crystal and

☆ Dedicated to Professor Kurt Merzweiler on the occasion of his 65th birthday.

* Corresponding author.
E-mail address: ruediger.seidel@pharmazie.uni-halle.de (R.W. Seidel).

https://doi.org/10.1016/j.molstruc.2023.137010
Received 20 July 2023; Received in revised form 15 October 2023; Accepted 3 November 2023
Available online 4 November 2023

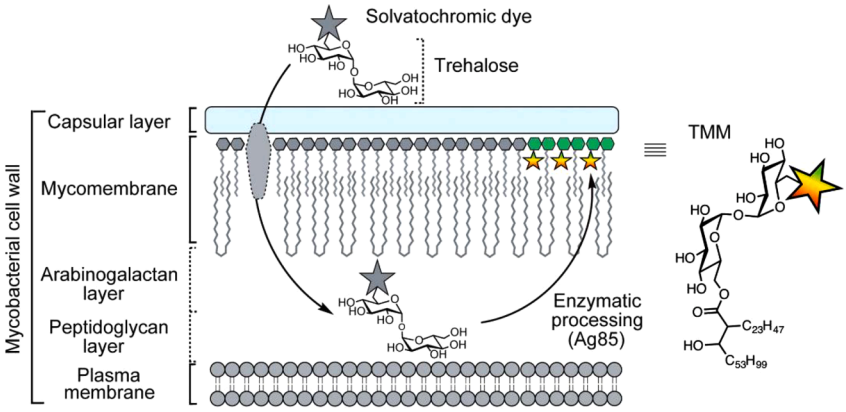

Fig. 1. Schematic representation of the mycobacterial cell wall, showing the transformation of dye trehalose conjugates to the analogous trehalose monomycolates (TMM, chemical diagram on the right) and incorporation into the mycomembrane. The figure was adapted from ref. [10]. Published Open Access under the Creative Commons Attribution 4.0 International License (https://creativecommons.org/licenses/by/4.0/ (accessed on 11 July 2023)). Copyright 2021 The Authors.

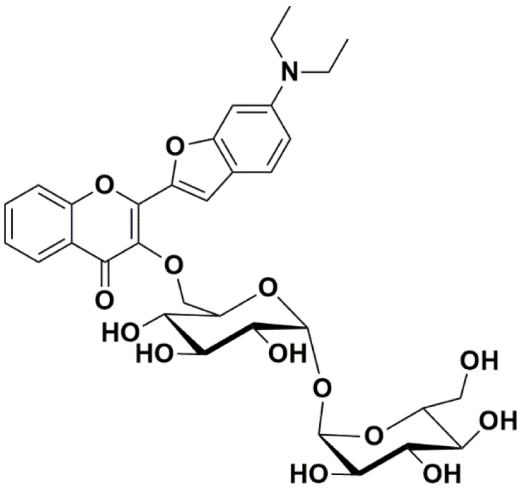

Fig. 2. Chemical diagram of **3HC-2-Tre**.

Table 1
Crystal data and refinement details for **3HC-2-Tre** · 3.14 H_2O.

Empirical formula	$C_{33}H_{39}NO_{17.14}$
M_r	723.89
T (K)	150(2)
λ (Å)	0.71073
Crystal system	Orthorhombic
Space group	$P2_12_12_1$
a (Å)	7.2371(3)
b (Å)	26.7785(12)
c (Å)	34.8048(15)
V (Å^3)	6745.1(5)
Z, Z'	8, 2
ρ (g cm^{-3})	1.426
μ (mm^{-1})	0.116
F(000)	3049
Crystal size (mm)	0.280 × 0.026 × 0.025
θ range (°)	1.91–25.00
Reflections collected / unique	525,500 / 11,893
R_{int}	0.2908
Observed data [$I > 2\sigma(I)$]	8554
Data / restraints / parameters	11,893 / 72 / 983
Goodness-of-fit on F^2	1.069
$R1$ [$I > 2\sigma(I)$]	0.0620
$wR2$ (all data)	0.1619
$\Delta\rho_{max}$, $\Delta\rho_{min}$ (e Å^{-3})	0.29, −0.22

molecular structure of the solvatochromic dye 2-(6-(diethyl-amino) benzofuran-2-yl)-3-hydroxy-4*H*-chromen-4-one (**3HC-2**) and preliminary labelling experiments with *Mycobacterium aurum*, a generally considered non-pathogenic mycobacterium and model organism used in antimycobacterial drug discovery, using the dye trehalose conjugate **3HC-2-Tre** (Fig. 2) [18]. We have now characterized **3HC-2-Tre** by X-ray crystallography and spectroscopic methods, and performed preliminary fluorescent labelling experiments with *Mycobacterium abscessus*. This NTM species has emerged as responsible for pulmonary infections with poor prognosis, particularly in patients with cystic fibrosis [19], and therefore has come into the focus of our drug discovery efforts [20,21].

2. Experimental section

2.1. General

The synthesis of **3HC-2-Tre** from **3HC-2** and anhydrous d-trehalose can be found in the literature [10,18]. Experimental details of the purification of **3HC-2-Tre** by preparative HPLC have been reported in the supplementary materials of ref. [18]. **3HC-2** was purified for the labelling experiment by recrystallization from acetonitrile [12]. Absorption spectra were acquired on a Thermo Scientific GENESYS 180 UV–visible Spectrophotometer, using quartz glass cuvettes (d = 1 cm). Solvents were of analytical grade.

2.2. X-ray crystallography

Crystals of **3HC-2-Tre** · 3.14 H_2O suitable for X-ray diffraction, albeit as extremely fine needles and consequently weakly diffracting, were obtained from a solution of **3HC-2-Tre** in methanol/water (2:1) by slow evaporation of the solvents at room temperature. Diffraction data with a redundancy of over 30 to increase the $I/\sigma(I)$ ratio were collected on a Bruker AXS D8 Venture diffractometer equipped with an Incoatec IμS microfocus X-ray source with Montel multilayer optics and a CMOS Photon III detector. The diffractometer was operated using the APEX4 software [22], and the diffraction images were processed with SAINT [23]. Scaling and a Gaussian absorption correction based on indexed crystal faces were carried out with SADABS [24]. The crystal structure was solved with SHELXT [25], using intensity data averaged and scaled assuming point group *mmm*, and refined with SHELXL-2019/3 [26]. For the final structure refinement, the intensity data were averaged and scaled applying 222 point group symmetry. An ethyl group, a hydroxymethyl group and one solvent water molecule were found to be disordered. Appropriate restraints on geometric parameters and atomic displacement parameters were applied to disordered regions (see

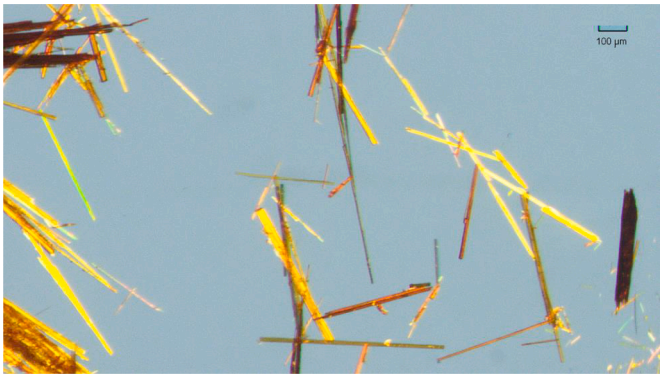

Fig. 3. Microscope image of needle-shaped crystals of **3HC-2-Tre** · 3.14 H_2O.

supplementary crystallographic data). In addition, the SWAT instruction in SHELXL was used to model diffuse solvent [27]. Hydrogen atoms of **3HC-2-Tre** were placed in geometrically calculated positions and refined using an appropriate riding model. Hydrogen atoms on the water molecules were poorly located in difference Fourier maps and were thus excluded from the structure refinement. The absolute structure was inferred from the known absolute configuration of the d-trehalose starting material used in the synthesis of **3HC-2-Tre**. Structure pictures were generated with Diamond [28] and Mercury [29]. The solvent area volume per unit cell volume was calculated with Platon [30], using default settings, and the Bravais–Friedel–Donnay–Harker (BFDH) morphology [31–33] with Mercury. Crystal data and refinement details are listed in Table 1.

2.3. Computational methods

The structure of the free molecule of **3HC-2-Tre** was optimized by DFT calculations with ORCA 5.0 [34], using a B3LYP functional [35,36] and a def2-TZVPP basis set [37]. The starting molecular structure was taken from the non-disordered molecule 1 in the crystal structure of **3HC-2-Tre** · 3.14 H_2O. The structures of methanol and 2-propanol hydrogen-bonded to the nitrogen atom of **3HC-2-Tre** were optimized in a similar manner from geometries created by Avogadro [38], using coordinates from the non-disordered molecule in the crystal structure and including an atom-pairwise dispersion correction to the DFT energy with Becke–Johnson damping [39] and an auxiliary basis def2/J [40]. The λ_{max} values for the UV–vis absorption bands were calculated using time-dependent DFT (TD-DFT) employed by ORCA 5.0, using the same B3LYP functional and def2-TZVPP basis set with 30 excited states including a conductor-like polarizable continuum solvent model (CPCM) for both the ground and the excited states [41]. Cartesian coordinates of the DFT-optimized structures of **3HC-2-Tre, 3HC-2-Tre** · CH_3OH and **3HC-2-Tre** · $(CH_3)_2CHOH$ can be found in the MOL file format in the Supplementary Materials.

2.4. Microbiology and fluorescence microscopy

The wild-type strain *M. abscessus* ATCC 19977 was cultivated by inoculation of a thawed glycerol stock (1 mL, see Supplementary Materials) into 10 mL of Middlebrook 7H9 liquid medium supplemented with 10 % ADS (5 % bovine serum albumin fraction V, 0.81 % sodium chloride, 2 % dextrose in purified water) and 0.05 % polysorbate 80. The liquid culture was grown to an OD_{600} between 0.2 and 0.8 by incubation at 37 °C in a humidified atmosphere of 5 % carbon dioxide with shaking. The culture was then diluted to 5×10^7 CFU mL^{-1} (OD_{600} = 0.1 is equivalent to 1×10^8 CFU mL^{-1}) with growth medium and 1 µL was transferred to a clear flat-bottom 96-well plate (Sarstedt, 83.3924.500) with 100 µL growth medium per well. After two days of incubation, 1 µL of **3HC-2-Tre** or **3HC-2** (10 mM in DMSO) was added to each well to

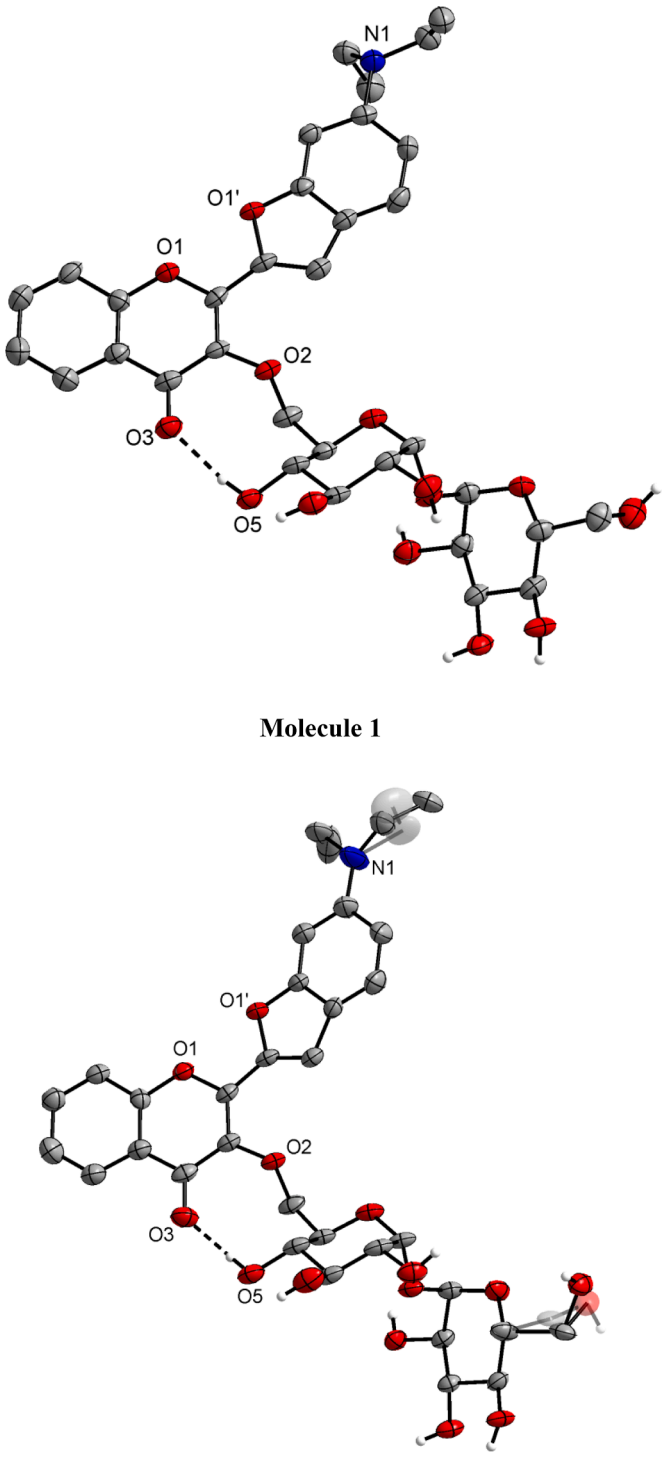

Fig. 4. Displacement ellipsoid plots (50 % probability level) of unique molecules 1 and 2 in the crystal structure of **3HC-2-Tre** · 3.14 H_2O. Hydrogen atoms are represented by small spheres of arbitrary radius. Carbon-bound hydrogen atoms are omitted for clarity. Dashed lines represent hydrogen bonds. Minor disorder parts in molecule 2 are shaded. Colour scheme: C, gray; H, white, N, blue; O, red. (For interpretation of the references to colour in this figure legend, the reader is referred to the web version of this article.)

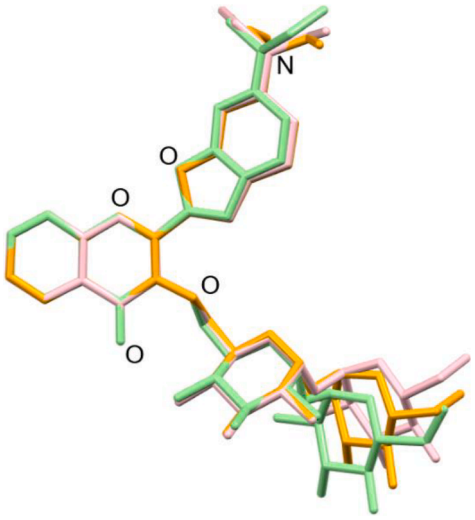

Fig. 5. Structure overlay plot of the unique **3HC-2-Tre** molecules 1 (green) and 2 (orange) in the crystal structure of **3HC-2-Tre** · 3.14 H_2O and the DFT-optimized structure of the free molecule (pink), superimposed at the non-hydrogen atoms of the chromone moieties. Hetero atoms of the chromophore are labelled with atom types for easy orientation. Disorder in molecule 2 and hydrogen atoms have been omitted for clarity. (For interpretation of the references to colour in this figure legend, the reader is referred to the web version of this article.)

achieve a final dye concentration of 100 μM. After homogenization by pipetting, the plate was incubated for three hours without shaking. Thereafter, the homogenization step was repeated and 1 μL of each well was transferred to a black clear flat-bottom 96-well plate (Greiner Bio-One, 6550909) filled with 200 μL of phosphate-buffered saline with 4 % paraformaldehyde per well. After fixation, fluorescence microscopy was carried out with a Thermo Scientific CellInsight CX5 instrument, exciting the sample at 485 nm and imaging with the GFP filter sets (510–531 nm).

3. Results and discussion

3.1. Structural elucidation

The dye trehalose conjugate **3HC-2-Tre** was prepared following the procedure reported by Kamariza et al. [10], as we described recently [18]. The final step of the elusive synthesis is shown in Fig. S1 in the Supplementary Materials. The compound was characterized by ^{1}H and ^{13}C NMR spectroscopy (Figs. S2 and S3), $^{1}H,^{13}C$ HSQC NMR (Figs. S4 and S5), high-resolution mass spectrometry (Fig. S6) and HPLC analysis (Fig. S7). Crystallization from a solution of **3HC-2-Tre** in methanol/-water afforded very thin needle-shaped crystals (Figs. 3 and S8). X-ray crystallography revealed the orthorhombic crystal structure of a 3.14 hydrate of **3HC-2-Tre**, which we discuss in the following paragraphs.

The crystal structure of **3HC-2-Tre** · 3.14 H_2O comprises two crystallography distinct molecules of **3HC-2-Tre** ($Z' = 2$) and 3.14 water

Table 2
Geometric parameters (Å, °) for selected hydrogen bonds in **3HC-2-Tre** · 3.14 H_2O. The numbers after the underscore indicate unique molecules 1 and 2 (cf. Fig. 6).

D—H···A	d(D···H)	d(H···A)	d(D···A)	<(DHA)
O5_1–H5A_1···O3_1	0.84	1.93	2.760(6)	171.3
O11_1-H11_1···O10_2	0.84	1.96	2.794(7)	169.4
O12_1-H12_1···O5_2	0.84	1.91	2.704(6)	156.0
O5_2-H5A_2···O3_2	0.84	1.89	2.728(7)	179.1
O11_2-H11_2···O10_1	0.84	1.90	2.718(7)	164.1
O12_2-H12_2···O5_1	0.84	2.02	2.763(6)	146.8

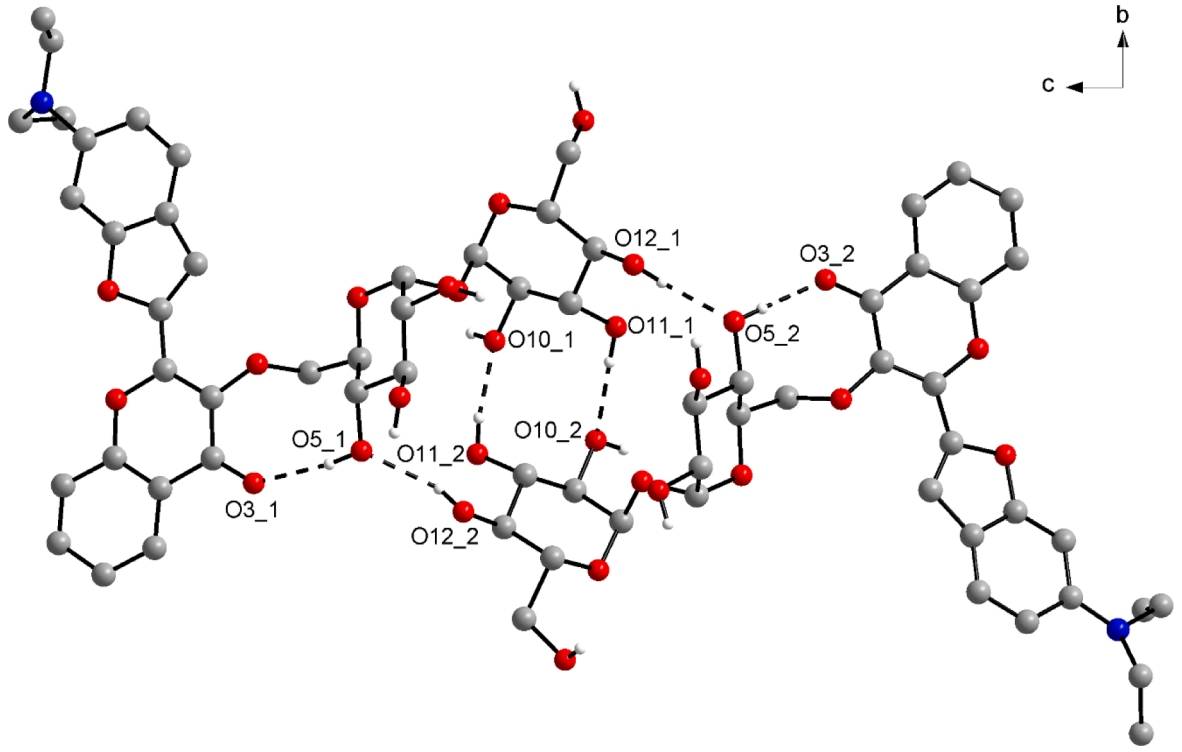

Fig. 6. Hydrogen-bonded assembly of unique molecules 1 and 2 (indicated by the number after the underscore) in the asymmetric unit of **3HC-2-Tre** · 3.14 H_2O, viewed along the *a* axis direction. Dashed lines represent hydrogen bonds. Disorder, carbon-bound hydrogen atoms and solvent water molecules are omitted for clarity. Colour scheme: C, gray; H, white; N, blue; O, red. (For interpretation of the references to colour in this figure legend, the reader is referred to the web version of this article.)

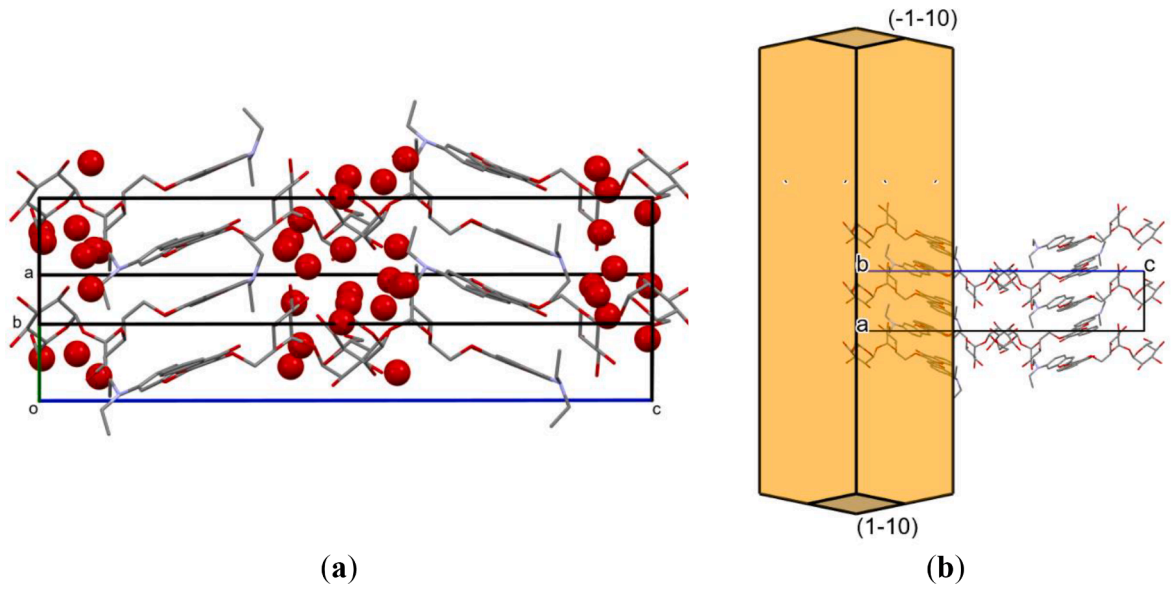

Fig. 7. (a) Part of the crystal structure of **3HC-2-Tre** · 3.14 H_2O, viewed along the [1-20] direction (water oxygen atoms shown with half atomic radius) and (b) viewed along the [010] direction with the calculated BFDH morphology (needle axis along the *a* axis direction; water molecules not shown). Disorder and hydrogen atoms have been omitted for clarity. Colour scheme: C, gray; N, blue; O, red. (For interpretation of the references to colour in this figure legend, the reader is referred to the web version of this article.)

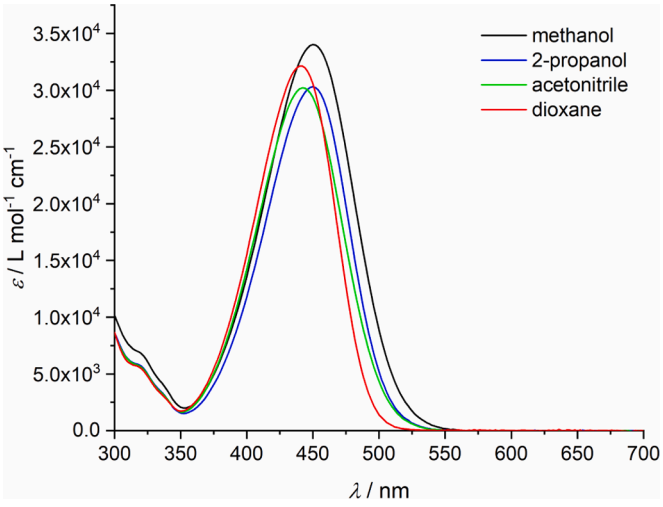

Fig. 8. Absorption spectra of **3HC-2-Tre** in different solvents (c = 25 μM).

Table 3
Experimental and theoretical (TD-DFT) UV–vis spectroscopic properties of **3-HC-2-Tre** in different solvents.

Solvent	λ_{max} / nm	λ_{max} / nm (TD-DFT)	+ H-bonded solvent	ε / 10^4 L mol^{-1} cm^{-1}
Methanol	450	464.8	446.4	3.40
2-Propanol	450	466.3	454.4	3.03
Acetonitrile	442	465.6	–	3.02
1,4-Dioxane	442	457.8	–	3.21

molecules per formula unit, based on refinement of the occupancy of one oxygen atom of water. Fig. 4 depicts the molecular structures of the two unique **3HC-2-Tre** molecules. Both molecules adopt an *s-cis* conformation about the C—C bond joining the chromone and benzofurane moieties like in the crystal structure of free **3HC-2** [18]. The chromophore in molecule 1 is nearly planar, apart from the two ethyl groups on the amine, with an angle between the mean planes through the 11-membered chromone system and the nine-membered benzofurane moiety of only 1.2(2)°. In molecule 2 the angle and thus the deviation from planarity is somewhat larger at 15.8(2)°. A prominent feature of the molecular structure of **3HC-2-Tre** is an intramolecular O—H···O hydrogen bond between the 5-hydroxy group of trehalose and the carbonyl oxygen atom of the chromone moiety, resulting in a nine-membered ring. The graph set descriptor is S(9) [42]. Similar intramolecular O—H···O hydrogen bonding interactions, albeit with an S(8) motif, between a flavone carbonyl oxygen atom and a sugar moiety appended to a 3-hydroxy group have been encountered previously [43–45]. Whereas there are currently 20 crystal structures featuring a 3-hydroxychromone unit bonded via a glycosidic bond at C1 of a pyranose ring in the Cambridge Structural Database [46], structures containing a chromone unit linked via C3 to C6 of a pyranose ring through an ether group have to our knowledge not been reported thus far. In molecule 1 in **3HC-2-Tre** · 3.14 H_2O, the nitrogen atom of the diethylamino group appears to act as a hydrogen bond acceptor for a water molecule with $d(D\cdots A)$ = 2.84 Å, and shows a slightly pyramidal coordination. In molecule 2, the diethylamino group of the chromophore and the 6′-hydroxymethyl group of trehalose are affected by disorder (Fig. 4, bottom), and no water molecule in hydrogen bond distance to the dimethylamino nitrogen atom is encountered. The orientation of the two glucose units to one another is similar to that observed in the crystal structures of anhydrous trehalose [47] and the dihydrate [48]. Fig. 5 shows a structure overlay plot of the chromone moieties of the two crystallographically unique molecules and that of the minimum energy structure of the free molecule (B3LYP/def2-TZVPP), and reveals that the structures differ mainly in the conformation of the dimethylamino group of the chromophore and the orientation of the terminal glucose residue.

In the crystal, the unique **3HC-2-Tre** molecules 1 and 2 form a hydrogen-bonded dimer, exhibiting approximate local C_2 point group symmetry with the C_2 axis oriented parallel to the crystallographic *a* axis direction (Fig. 6). The molecules are joined by four intermolecular O—H···O hydrogen bonds established between the trehalose moieties, with the exclusion of solvent water molecules. The graph set descriptor for the central ten-membered ring motif formed by the hydrogen bonds between O11 and O10 of each molecule is $R_2^2(10)$ [42], and that for the larger ring formed through O5 and O12 is $R_2^2(24)$. Table 2 lists the

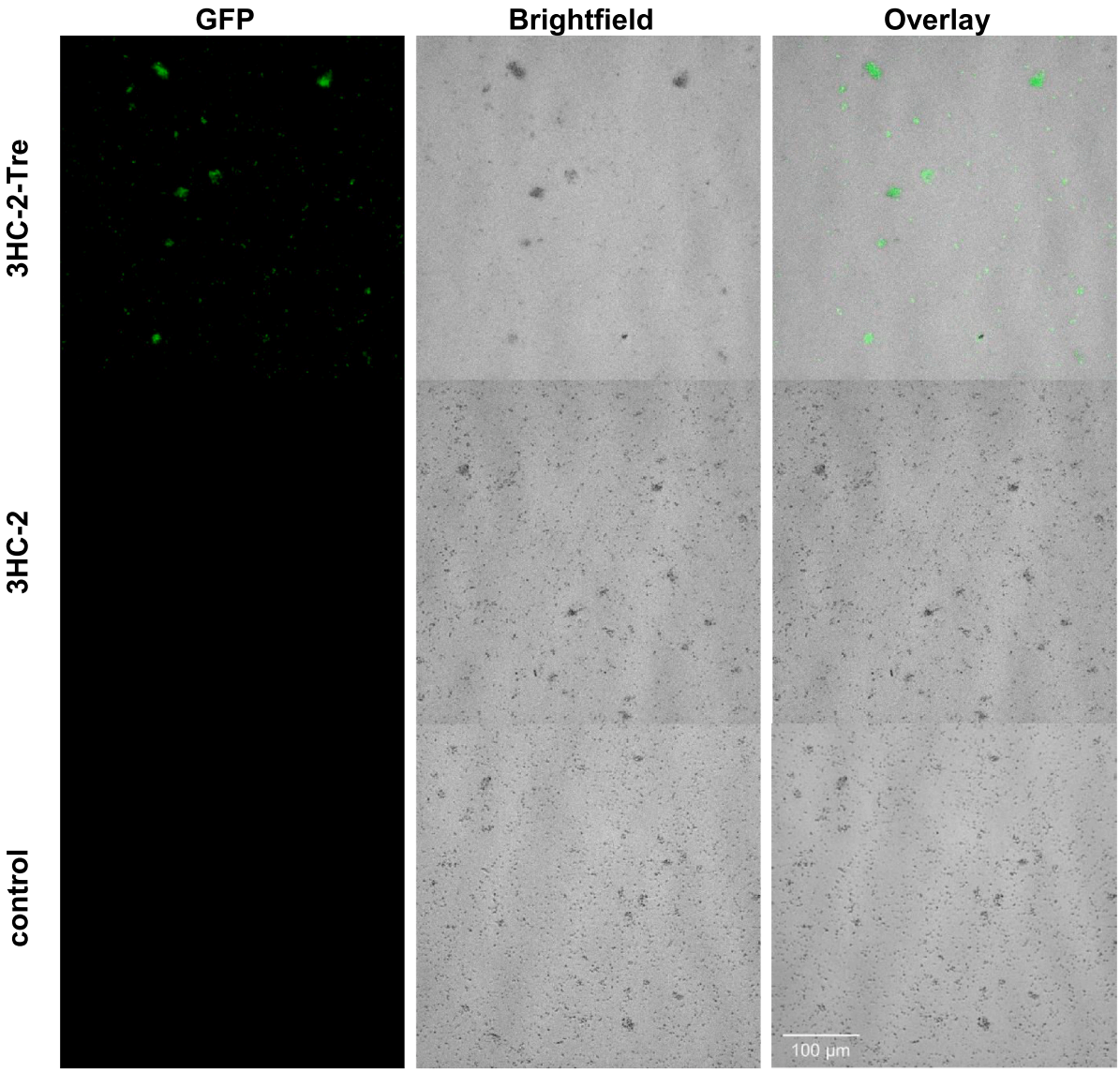

Fig. 9. Microscope imaging (20× magnification) of *M. abscessus* cells incubated with 100 µM **3HC-2-Tre** and 100 µM **3HC-2** as well as untreated cells as control (GFP channel: λ_{ex} = 485 nm, λ_{em} = 510–531 nm). The images are exposure time and gain matched.

corresponding geometric hydrogen bond parameters, which are as expected for strong O—H···O hydrogen bonds [49]. Fig. 7a shows part of a packing diagram of the structure of **3HC-2-Tre** · 3.14 H_2O, revealing hydrophilic and hydrophobic regions in the crystal. The hydrophilic regions in crystal feature hydrogen-bonded trehalose moieties and solvent water molecules. The latter occupy approximately 7.4 % of the unit cell volume, and are localized around the trehalose units. The hydrophobic regions are dominated by π···π stacking interactions of the chromophore. The BFDH morphology calculated for **3HC-2-Tre** · 3.14 H_2O (Fig. 7b) suggests that the stacking of the chromophore moieties determines the needle shape [100] of the crystals (Figs. 3 and S8).

3.2. *UV–vis spectroscopic properties*

Klymchenko et al. studied absorption and fluorescence properties of the free dye **3HC-2** and related 3-hydroxychromones in detail [11,12], and Kamariza et al. characterized fluorescence properties of **3HC-2-Tre** and related dye trehalose conjugates in 1,4-dioxane / water solvent systems [10]. Since we were not aware of a literature report of absorption properties of the dye trehalose conjugate **3HC-2-Tre**, we recorded UV–vis spectra of the compound in four different solvents (Fig. 8) and compared the results with those obtained from time-dependent TD-DFT calculations (Table 3). In the non-polar ether solvent 1,4-dioxane and in the polar aprotic solvent acetonitrile, the absorption maximum is centred at 442 nm in the visible region. A slight bathochromic shift of 8 nm is observed in the polar protic solvents methanol and 2-propanol. The positions of the absorption maxima and the observed small positive solvatochromy of **3HC-2-Tre** are comparable with the absorption properties of unbound **3HC-2**, whereas high fluorescence sensitivity to solvents is known for both **3HC-2** [11,12] and **3HC-2-Tre** [10].

TD-DFT calculations on **3HC-2-Tre** predicted the absorption maxima roughly correctly (Table 3). The largest difference between experimental and calculated absorption maximum is observed for acetonitrile. This can possibly be ascribed to the fact that hydrogen bonding and dipole-dipole interactions between solute and solvent are not properly taken into account by the TD-DFT method with an implicit solvent model. The presence of a water oxygen atom in hydrogen bond distance to a slightly pyramidal diethylamino nitrogen atoms in the crystal structure of **3HC-2-Tre** · 3.14 H_2O (*vide supra*) suggests that this group could also act as hydrogen acceptor in protic solvents. Indeed, the inclusion of one molecule of methanol or 2-propanol hydrogen-bonded to

the diethylamino group of **3HC-2-Tre** (Fig. S9) considerably improved the agreement between experiment and theory (column 3 in Table 3).

3.3. Fluorescent labelling of Mycobacterium abscessus cells

In order to investigate whether *M. abscessus* cells can be fluorescently labelled using **3HC-2-Tre**, we incubated a wild-type strain in liquid growth medium in the presence of 100 μM **3HC-2-Tre**, following a protocol similar to that we had successfully applied for fluorescent labelling of *M. aurum* cells using the same dye trehalose conjugate [18]. Our preliminary results depicted in Fig. 9 indicate fluorescence of *M. abscessus* cells labelled with **3HC-2-Tre** when excited at $\lambda_{ex} = 485$ nm and imaged with the GFP channel ($\lambda_{em} = 510–531$ nm), similar to our previous observations for *M. aurum* [18].

It is worth noting that Kamariza et al. arrived at the conclusion that **3HC-2-Tre**-labelling of *Mycobacterium smegmatis* cells, a generally considered non-pathogenic mycobacterial strain and surrogate bacterium for the pathogen *M. tuberculosis* [50], is not specific to the trehalose pathway, in contrast to the derivative named **3HC-3-Tre** (bearing a 9, 9-dimethyl-9*H*-fluorene group instead of the benzofuran moiety in **3HC-2-Tre**) [10]. Whether this applies to mycobacterial species in general, and the exact mechanism of **3HC-2-Tre**-labelling have not yet been explored to our knowledge. To shed some light on this, we also subjected *M. abscessus* cells incubated with unbound **3HC-2** and untreated cells as control to fluorescence microscopy. Essentially no fluorescence was detected for **3HC-2**-treated and untreated cells with the GFP channel (Fig. 9). This suggests that fluorescence labelling depends on trehalose in the wild-type *M. abscessus* strain used in this case.

Whereas much work has been done on fluorescent labelling of *M. tuberculosis* cells using trehalose-based probes [10,13-16], we are not aware of related studies on labelling of *M. abscessus* cells. Sarrazin et al., however, demonstrated that cyclipostins and cyclophostin derivatives containing a fluorescent dansyl group are efficient probes that specifically label a variety of mycobacterial species, including *M. abscessus* [51].

4. Conclusions

3HC-2-Tre · 3.14 H_2O appears to be the first crystal structure determination of a chromophore attached to trehalose. The preferred *s-cis* conformation of the dye **3HC-2** is retained in the trehalose conjugate. The crystal structure containing two unique **3HC-2-Tre** molecules ($Z' = 2$) features intra- and intermolecular O—H···O hydrogen bonds. Absorption spectroscopy showed small positive solvatochromy for **3HC-2-Tre**, similar to the unbound dye. The inclusion of one molecule of methanol or 2-propanol hydrogen-bonded to the diethylamino group of **3HC-2-Tre** in the TD-DFT calculations improved the agreement between measured and calculated absorption maxima. This suggests that the diethylamino group in solution likely acts as hydrogen bond acceptor for protic solvents, in analogy to the possible O_{water}—H···N_{amine} hydrogen bonding interaction encountered in the solid structure of **3HC-2-Tre** · 3.14 H_2O. Our preliminary investigations show that *M. abscessus* cells can be detected with fluorescence microscopy in the GFP channel after incubation with **3HC-2-Tre** and suggest that the mechanism of labelling is trehalose-dependent in this case. We envisage that **3HC-2-Tre**-labelling could be a useful tool for in vitro drug susceptibility testing against this opportunistic pathogen.

CRediT authorship contribution statement

Adrian Richter: Conceptualization, Methodology, Investigation, Resources, Writing – review & editing, Visualization, Supervision, Project administration, Funding acquisition. **Richard Goddard:** Conceptualization, Methodology, Validation, Formal analysis, Investigation, Resources, Data curation, Writing – review & editing, Visualization. **Lea Mann:** Methodology, Investigation, Writing – review & editing, Visualization. **Fabienne Siersleben:** Methodology, Investigation, Funding acquisition. **Rüdiger W. Seidel:** Conceptualization, Methodology, Validation, Formal analysis, Investigation, Data curation, Writing – original draft, Visualization, Project administration.

Declaration of Competing Interest

The authors declare that they have no known competing financial interests or personal relationships that could have appeared to influence the work reported in this paper.

Data availability

CCDC 2283026 contains the supplementary crystallographic data for this paper. The data can be obtained free of charge from the Cambridge Crystallographic Data Centre via www.ccdc.cam.ac.uk/structures.

Acknowledgements

We would like to thank Professor Christian W. Lehmann for providing access to the X-ray diffraction facility at the Max-Planck-Institut für Kohlenforschung and Heike Schucht for technical assistance with the X-ray intensity data collection. Thanks are also due to Dr. Christian Ihling and Antje Herbrich-Peters for performing the high-resolution mass spectrometry. This work was funded by the Deutsche Forschungsgemeinschaft (DFG, German Research Foundation) - 432291016 (to A.R.), Mukoviszidose Institut gGmbH (Bonn, Germany) project number 2202 (to A.R.), the research and development arm of the German Cystic Fibrosis Association Mukoviszidose e. V., and by a scholarship from the Vereinigung der Freunde und Förderer des Institutes für Pharmazie der Martin-Luther-Universität Halle-Wittenberg (VFFIP) to F.S.

Supplementary materials

Supplementary material associated with this article can be found, in the online version, at doi:10.1016/j.molstruc.2023.137010.

References

[1] Global Tuberculosis Report 2022, World Health Organization, Geneva, 2022.
[2] S.H.E. Kaufmann, U.E. Schaible, 100th anniversary of Robert Koch's Nobel Prize for the discovery of the tubercle bacillus, Trends Microbiol. 13 (2005) 469–475.
[3] A. Sharma, M. De Rosa, N. Singla, G. Singh, R.P. Barnwal, A. Pandey, Tuberculosis: an overview of the immunogenic response, disease progression, and medicinal chemistry efforts in the last decade toward the development of potential drugs for extensively drug-resistant tuberculosis strains, J. Med. Chem. 64 (2021) 4359–4395.
[4] S.S.R. Alsayed, H. Gunosewoyo, Tuberculosis: pathogenesis, current treatment regimens and new drug targets, Int. J. Mol. Sci. 24 (2023) 5202.
[5] V.N. Dahl, M. Molhave, A. Floe, J. van Ingen, T. Schön, T. Lillebaek, A.B. Andersen, C. Wejse, Global trends of pulmonary infections with nontuberculous mycobacteria: a systematic review, Int. J. Infect. Dis. 125 (2022) 120–131.
[6] Y.M. Wi, Treatment of extrapulmonary nontuberculous mycobacterial diseases, Infect. Chemother. 51 (2019) 245–255.
[7] E. Ricotta, J. Adjemian, R. Blakney, Y.L. Lai, S. Kadri, D.R. Prevots, Extrapulmonary nontuberculous mycobacteria infections in hospitalized patients, United States, 2009–2014, Emerg. Infect. Dis. 27 (2021) 845–852.
[8] M.R. Loebinger, J.K. Quint, R. van der Laan, M. Obradovic, R. Chawla, A. Kishore, J. van Ingen, Risk factors for nontuberculous mycobacterial pulmonary disease: a systematic literature review and meta-analysis, Chest 164 (2023) 1115–1124.
[9] R. Singhal, V.P. Myneedu, Microscopy as a diagnostic tool in pulmonary tuberculosis, Int. J. Mycobacteriol. 4 (2015) 1–6.
[10] M. Kamariza, S.G.L. Keyser, A. Utz, B.D. Knapp, C. Ealand, G. Ahn, C.J. Cambier, T. Chen, B. Kana, K.C. Huang, C.R. Bertozzi, Toward point-of-care detection of mycobacterium tuberculosis: a brighter solvatochromic probe detects mycobacteria within minutes, JACS Au 1 (2021) 1368–1379.
[11] A.S. Klymchenko, T. Ozturk, V.G. Pivovarenko, A.P. Demchenko, A 3-hydroxychromone with dramatically improved fluorescence properties, Tetrahedron Lett. 42 (2001) 7967–7970.

[12] A.S. Klymchenko, V.G. Pivovarenko, T. Ozturk, A.P. Demchenko, Modulation of the solvent-dependent dual emission in 3-hydroxychromones by substituents, New J. Chem. 27 (2003) 1336–1343.
[13] N. Banahene, D.M. Gepford, K.J. Biegas, D.H. Swanson, Y.-P. Hsu, B.A. Murphy, Z. E. Taylor, I. Lepori, M.S. Siegrist, A. Obregón-Henao, M.S. Van Nieuwenhze, B. M. Swarts, A far-red molecular rotor fluorogenic trehalose probe for live mycobacteria detection and drug-susceptibility testing, Angew. Chem. Int. Ed. 62 (2023), e202213563.
[14] H.A. Sahile, C. Rens, T. Shapira, R.J. Andersen, Y. Av-Gay, DMN-Tre labeling for detection and high-content screening of compounds against intracellular mycobacteria, ACS Omega 5 (2020) 3661–3669.
[15] T. Dai, J. Xie, Q. Zhu, M. Kamariza, K. Jiang, C.R. Bertozzi, J. Rao, A fluorogenic trehalose probe for tracking phagocytosed mycobacterium tuberculosis, J. Am. Chem. Soc. 142 (2020) 15259–15264.
[16] G. Kumar, R. Narayan, S. Kapoor, Chemical tools for illumination of tuberculosis biology, virulence mechanisms, and diagnosis, J. Med. Chem. 63 (2020) 15308–15332.
[17] N. Banahene, B.M. Swarts, Metabolic labeling of live mycobacteria with trehalose-based probes, in: T. Parish, A. Kumar (Eds.), Mycobacteria Protocols, Springer US, New York, NY, 2021, pp. 385–398.
[18] A. Richter, R. Goddard, F. Siersleben, L. Mann, R.W. Seidel, Structural elucidation of 2-(6-(diethylamino)benzofuran-2-yl)-3-hydroxy-4*H*-chromen-4-one and labelling of mycobacterium aurum cells, Molbank 2023 (2023) M1647.
[19] Y.M. Boudehen, L. Kremer, *Mycobacterium abscessus*, Trends Microbiol. 29 (2021) 951–952.
[20] L. Mann, U.S. Ganapathy, R. Abdelaziz, M. Lang, M.D. Zimmerman, V. Dartois, T. Dick, A. Richter, In vitro profiling of the synthetic RNA polymerase inhibitor MMV688845 against *Mycobacterium abscessus*, Microbiol. Spectr. 10 (2022), e0276022.
[21] M. Lang, U.S. Ganapathy, L. Mann, R. Abdelaziz, R.W. Seidel, R. Goddard, I. Sequenzia, S. Hoenke, P. Schulze, W.W. Aragaw, R. Csuk, T. Dick, A. Richter, Synthesis and characterization of phenylalanine amides active against *Mycobacterium abscessus* and other Mycobacteria, J. Med. Chem. 66 (2023) 5079–5098.
[22] APEX4, Bruker AXS Inc, Madison, Wisconsin, USA, 2017.
[23] SAINT V8.40B, Bruker AXS Inc., Madison, Wisconsin, USA, 2019.
[24] SADABS, Bruker AXS Inc., Madison, Wisconsin, USA, 2012.
[25] G.M. Sheldrick, SHELXT - integrated space-group and crystal-structure determination, Acta Crystallogr. A 71 (2015) 3–8.
[26] G.M. Sheldrick, Crystal structure refinement with SHELXL, Acta Crystallogr. C 71 (2015) 3–8.
[27] P.C. Moews, R.H. Kretsinger, Refinement of the structure of carp muscle calcium-binding parvalbumin by model building and difference Fourier analysis, J. Mol. Biol. 91 (1975) 201–225.
[28] K. Brandenburg, Diamond, Crystal Impact GbR, Bonn, Germany, 2018.
[29] C.F. Macrae, I. Sovago, S.J. Cottrell, P.T.A. Galek, P. McCabe, E. Pidcock, M. Platings, G.P. Shields, J.S. Stevens, M. Towler, P.A. Wood, Mercury 4.0: from visualization to analysis, design and prediction, J. Appl. Crystallogr. 53 (2020) 226–235.
[30] A.L. Spek, Structure validation in chemical crystallography, Acta Crystallogr. D 65 (2009) 148–155.
[31] A. Bravais, Etudes Cristallographiques, Gauthier-Villars, Paris, 1866.
[32] G. Friedel, Etudes sur la loi de Bravais, Bull. Soc. Fr. Miner. 30 (1907) 326–455.
[33] J.D.H. Donnay, D. Harker, A new law of crystal morphology extending the law of Bravais, Am. Miner. 22 (1937) 446–467.
[34] F. Neese, F. Wennmohs, U. Becker, C. Riplinger, The ORCA quantum chemistry program package, J. Chem. Phys. 152 (2020), 224108.
[35] A.D. Becke, Density-functional thermochemistry. III. The role of exact exchange, J. Chem. Phys. 98 (1993) 5648–5652.
[36] C. Lee, W. Yang, R.G. Parr, Development of the Colle–Salvetti correlation-energy formula into a functional of the electron density, Phys. Rev. B 37 (1988) 785–789.
[37] F. Weigend, R. Ahlrichs, Balanced basis sets of split valence, triple zeta valence and quadruple zeta valence quality for H to Rn: design and assessment of accuracy, Phys. Chem. Chem. Phys. 7 (2005) 3297–3305.
[38] M.D. Hanwell, D.E. Curtis, D.C. Lonie, T. Vandermeersch, E. Zurek, G.R. Hutchison, Avogadro: an advanced semantic chemical editor, visualization, and analysis platform, J. Cheminform. 4 (2012) 17.
[39] S. Grimme, J. Antony, S. Ehrlich, H. Krieg, A consistent and accurate ab initio parametrization of density functional dispersion correction (DFT-D) for the 94 elements H-Pu, J. Chem. Phys. (2010) 132.
[40] F. Weigend, Accurate Coulomb-fitting basis sets for H to Rn, Phys. Chem. Chem. Phys. 8 (9) (2006) 1057–1065.
[41] V. Barone, M. Cossi, Quantum calculation of molecular energies and energy gradients in solution by a conductor solvent model, J. Phys. Chem. A 102 (1998) 1995–2001.
[42] J. Bernstein, R.E. Davis, L. Shimoni, N.L. Chang, Patterns in hydrogen bonding: functionality and graph set analysis in crystals, Angew. Chem. Int. Ed. 34 (1995) 1555–1573.
[43] G.-Z. Jin, Y. Yamagata, K.-i. Tomita, Structure of rutin pentamethanol, Chem. Pharm. Bull. 38 (1990) 297–300.
[44] I. da Silva, J.G. Díaz, J. González-Platas, Structure determination of monohydrated trifolin (Kaempferol 3-O-β-D-galactopyranoside) from laboratory powder diffraction data, J. Pharm. Sci. 100 (2011) 1588–1593.
[45] A. Sosa, C. Rosquete, J. Bruno, L. Rojas, L. Pouysegu, S. Quideau, J.-M. Leger, S. Massip, M.-A. Lacaille-Dubois, A.-C. Mitaine-Offer, Crystal structure analysis of 6,7-di-*O*-methyl-quercetagetin-3-O-β-D-glucopyranoside dihydrate isolated from *Urena sinuata* L, Av. Quim. 6 (2011) 55–59.
[46] C.R. Groom, I.J. Bruno, M.P. Lightfoot, S.C. Ward, The Cambridge structural database, Acta Crystallogr. B 72 (2016) 171–179.
[47] G.A. Jeffrey, R. Nanni, The crystal structure of anhydrous α,α-trehalose at −150°, Carbohydr. Res. 137 (1985) 21–30.
[48] G.M. Brown, D.C. Rohrer, B. Berking, C.A. Beevers, R.O. Gould, R. Simpson, The crystal structure of α,α-trehalose dihydrate from three independent X-ray determinations, Acta Crystallogr. Sect. B 28 (1972) 3145–3158.
[49] R. Thakuria, B. Sarma, A. Nangia, 7.03—Hydrogen bonding in molecular crystals, in: J.L. Atwood (Ed.), Comprehensive Supramolecular Chemistry II, Elsevier, Oxford, 2017, pp. 25–48.
[50] J.A.T. Sundarsingh, J. Ranjitha, A. Rajan, V. Shankar, Features of the biochemistry of Mycobacterium smegmatis, as a possible model for Mycobacterium tuberculosis, J. Infect. Public Health 13 (2020) 1255–1264.
[51] M. Sarrazin, B.P. Martin, R. Avellan, G.R. Gnawali, I. Poncin, H.Le Guenno, C. D. Spilling, J.-F. Cavalier, S. Canaan, Synthesis and biological characterization of fluorescent cyclipostins and cyclophostin analogues: new insights for the diagnosis of mycobacterial-related diseases, ACS Infect. Dis. 8 (2022) 2564–2578.